Theoretical study of CeO_2 doped with tetravalent ions

D. A. Andersson,[1] S. I. Simak,[2] N. V. Skorodumova,[3] I. A. Abrikosov,[2] and B. Johansson[1,3]
[1]*Applied Materials Physics, Department of Materials Science and Engineering, Royal Institute of Technology, SE-100 44 Stockholm, Sweden*
[2]*Department of Physics, Chemistry, and Biology (IFM), Linköping University, SE-581 83 Linköping, Sweden*
[3]*Condensed Matter Theory Group, Department of Physics, Uppsala University, Box 530, SE-751 21 Uppsala, Sweden*
(Received 21 April 2007; revised manuscript received 2 August 2007; published 29 November 2007)

We have used density functional theory calculations within the LDA+U formulation to investigate how small amounts of dissolved SiO_2, GeO_2, SnO_2, or PbO_2 affect the redox thermodynamics of ceria (CeO_2). Compared to pure ceria, reduction is facilitated and the reducibility increases in the sequence of CeO_2-SnO_2, CeO_2-GeO_2, and CeO_2-SiO_2, which correlates with the decrease of the ionic radii of the solutes. For low solute concentrations, there is an inverse relation between high reducibility and the solution energy of tetravalent solutes. CeO_2-PbO_2 is unique in the sense that the initial reduction occurs by Pb(IV)⇒Pb(II) instead of the usual Ce(IV)⇒Ce(III) reaction. Among the investigated ceria compounds, CeO_2-PbO_2 has the lowest reduction energy and rather low solution energy. We have studied how the solution and reduction energies depend on the concentration of Si, Ge, Sn, Pb, Ti, Zr, Hf, and Th solute ions. While the solution energy increases monotonously with concentration, the reduction energy first decreases, as compared to pure ceria (except for Th, which exhibits a small increase), and with further increase of solute concentration, it either remains almost constant (Zr, Hf, and Th) or slightly increases (Ti, Si, Ge, and Sn).

DOI: 10.1103/PhysRevB.76.174119 PACS number(s): 61.72.Ji, 61.72.Ww, 66.10.Ed, 67.40.Yv

I. INTRODUCTION

Ceria based materials are found in a wide range of applications, for example, ceria-zirconia mixed oxides ($Ce_{1-y}Zr_yO_2$) are used for oxygen storage (release) in three-way catalysts for automotive exhaust treatment.[1,2] CeO_2 doped with divalent or trivalent ions is a promising electrolyte material for application in solid oxide fuel cells.[3–5] In three-way catalysts, ceria is used to control the oxygen atmosphere by making use of the ability of ceria to release oxygen by forming oxygen vacancies under reducing conditions and, conversely, to store oxygen by filling oxygen vacancies under oxidizing conditions. The excellent oxygen storage capacity (OSC) is an inherent property of ceria in the cubic fluorite structure.[6] The addition of ZrO_2 further improves the OSC as well as the thermal stability.[2,7–10] Using density functional theory (DFT) calculations, we have previously investigated how small amounts of tetravalent ions from group 4b in the Periodic Table, i.e., Zr^{4+}, Hf^{4+}, Ti^{4+}, and Th^{4+}, influence the redox thermodynamics and kinetics of ceria.[11] We concluded that reduction is facilitated by dissolving TiO_2 (largest improvement), HfO_2, or ZrO_2 (least improvement), while ThO_2 makes the reduction slightly more difficult. The migration barrier for the diffusion of oxygen ions is much lower in the neighborhood of a Ti ion (largest decrease), Hf ion, or Zr ion (least decrease), which increases the rate of oxygen diffusion. The binding energy of vacancies and solutes, which decreases from Ti, Hf, Zr, to Th, influences diffusion in the opposite direction by increasing the activation energy for diffusion. In Ref. 11, we rationalized the properties of ceria solid solutions in terms of defect cluster relaxations that are coupled to a gain in the band energy. Small ions such as Ti^{4+} enable a favorable relaxation pattern that allows large Ce^{3+} ions to fit into the ceria matrix, while large ions such as Th^{4+} instead worsen these properties. The benefits of dissolving ZrO_2 into CeO_2 are well established,[2,7–10] but HfO_2 (Ref. 12) and TiO_2 (Refs. 13 and 14) have also been identified as promising alternatives. Recent experiments[15,16] have reported a considerable decrease of the reduction energy for $Ce_{1-y}Zr_yO_2$ ($y=0.19$) compared to CeO_2, which is in agreement with our theoretical predictions in Ref. 11. Nevertheless, experiments suggest a slightly larger decrease than theory.[15,16] In conjunction with Ti, Zr, Hf, and Th, the group 4a elements, i.e., Si, Ge, Sn, and Pb, form tetravalent oxygen compounds and prospectively they can be used as solutes or dopants to optimize the properties of ceria. Moreover, Si is one of the main contaminants in commercial CeO_2 grades and thus it is important to understand its effect on redox thermodynamics and structural properties. Solid solutions of ceria and tetravalent ions from group 4a have only been scarcely discussed in the literature. One reason for this is the difficulty of forming the solid solutions in a controlled way. A few studies have been undertaken on composite and mixed CeO_2-SiO_2 (Refs. 17–20) materials, which under certain conditions were reported to possess favorable redox properties compared to pure CeO_2 and CeO_2-ZrO_2 mixed oxides. Due to the high complexity of these materials, interpretation of experiments is often nontrivial but could be made easier if the redox properties of the constituent phases were established. CeO_2-SnO_2 materials were studied by Lin *et al.*[21,22] and they found excellent redox properties and high catalytic activity. The development of new OSC materials will benefit from better knowledge of the redox properties and the stability ranges of CeO_2-MO_2 (M=Ti, Zr, Hf, Th, Si, Ge, Sn, or Pb) solution phases.

In the present paper, we address the above issues using theoretical methods based on the density functional theory. The details are described in Sec. II. We study small amounts of group 4a elements in ceria (Sec. III A–III C), as well as

the properties of $Ce_{1-y}M_yO_2$ (M=Si, Ge, Sn, Pb, Ti, Zr, Hf, and Th) solution phases in the solute range of $0 \leqslant y \leqslant 0.25$ (Sec. III D).

II. THEORY

The DFT calculations were performed with the Vienna *ab initio* simulation package (VASP) in the framework of the projector augmented wave method.[23–27] In order to account for the strong on-site Coulomb repulsion among the Ce $4f$ electrons, we have applied the LDA+U scheme formulated by Dudarev *et al.*[28] The exchange-correlation effects were treated within the local density approximation (LDA) together with a Hubbard U parameter of 6 eV since that is a good choice to describe the structural, electronic (band structure), and energetic properties of CeO_2, Ce_2O_3, and CeO_{2-x}.[29] We modeled defect properties using a $2\times2\times2$ supercell (96 sites), derived from the ideal fluorite structure. For small solute concentrations, the volume of the supercell was set equal to the calculated volume of pure ceria.[29] This results in an underestimation of the vacancy formation energy (see below) by 0.04–0.05 eV (1.4%–1.6%), which is negligible on the scale of vacancy formation energy values. This range was estimated through the volume relaxation of $CeO_{1.9688}$, $Ce_{1.9688}Ti_{0.0312}O_{1.9688}$, and $Ce_{1.9688}Si_{0.0312}O_{1.9688}$, as well as of the corresponding oxidized compounds, i.e., $Ce_{1.9688}Ti_{0.0312}O_2$ and $Ce_{1.9688}Si_{0.0312}O_2$. It is more important to include volume relaxation for high solute concentrations and, in our case, it was included for y=0.25. All internal structural parameters were relaxed until the Hellman-Feynman forces on each ion were negligible (<0.02 eV/Å). We used a plane-wave cutoff energy of 400 eV and applied a $2\times2\times2$ Monkhorst-Pack k-point mesh[30] (four irreducible k points) with Gaussian smearing of 0.20 eV.[29] For accurate calculation of the electronic density of states (DOS), we applied a $3\times3\times3$ k-point mesh[30] (eight irreducible k points) and the modified tetrahedron method of Blöchl.[31] All the band structure properties were derived from the accurate DOS calculations, but to improve visibility of atomiclike peaks, a smearing was also applied to all the DOS plots.

III. RESULTS AND DISCUSSION

A. Vacancy formation in $Ce_{0.9688}M_{0.0312}O_2$

Ceria releases oxygen according to the reaction

$$CeO_2 \Leftrightarrow CeO_{2-x} + \frac{x}{2}O_2. \quad (1)$$

The equilibrium is controlled by the oxygen chemical potential and for a given x, it is determined by

$$H_f^v - TS_f^v + \frac{RT}{2}\ln(P_{O_2}) = 0. \quad (2)$$

Here, P_{O_2} is the partial pressure of O_2, T is the temperature, and R is the molar gas constant. The vacancy formation enthalpy (H_f^v) and entropy (S_f^v) are defined as

$$X_f^v = \frac{1}{x}X_{CeO_{2-x}} + \frac{1}{2}X_{O_2} - \frac{1}{x}X_{CeO_2}, \quad (3)$$

where X denotes either enthalpy (H) or entropy (S). We assume that H_f^v is equal to the vacancy formation energy, E_f^v. Low E_f^v means high reducibility, which translates into a high OSC. Theoretical values of E_f^v derived from DFT calculations are underestimated compared to experiments.[29,32] By creating one vacancy in the $2\times2\times2$ supercell (x=0.0312), we estimate E_f^v to be 3.61 eV,[29] to be compared with measured values of 4.65–5.00 eV for bulk reduction.[33] The theoretical underestimation is largely due to the overestimation of the O_2 binding energy within DFT[29,31] (≈1.2 eV/0.5 O_2 in the LDA) and consequently the underestimation is independent of the conditions in the ceria material itself and can easily be corrected.

When a vacancy is formed in pure ceria, two electrons localize on two f-level traps on two nearest neighbor (NN) Ce ions, thus transforming into Ce^{3+}. This process is influenced by the presence of +4 solute ions. In Ref. 11, we identified an almost linear dependence of E_f^v on the ionic radius of the +4 solutes from group 4b, which is illustrated in Fig. 1(a) where these data have been reproduced. In this paper, the ionic radius[34] either refers to eightfold (Ti^{4+}, Zr^{4+}, Hf^{4+}, Th^{4+}, Sn^{4+}, and Pb^{4+}) or fourfold (Si^{4+} and Ge^{4+}) coordination of the tetravalent ions. Si^{4+} and Ge^{4+} strongly prefer fourfold rather than eightfold coordination and consequently there is no data for the ionic radius of the eightfold coordination. One may assume that the +4 ions from group 4a should follow a similar pattern; however, Fig. 1(a), at least partly, does not support this reasoning. The differences between the group 4a and 4b ions must originate from the electronic structure of the solid solutions.

According to Fig. 1(a), the vacancy formation energy in $Ce_{0.9688}Si_{0.0312}O_2$ is higher than the extrapolation from the group 4b elements; however, the absolute value is still somewhat lower than for $Ce_{0.9688}Ti_{0.0312}O_2$, which has the smallest vacancy formation energy of the group 4b ceria compounds. The explanation for the facile vacancy formation in $Ce_{0.9688}Si_{0.0312}O_2$ is that the small size of the Si^{4+} ions enables the large Ce^{3+} ions in reduced ceria to better fit into the ceria matrix. This is directly visible in the Ce^{3+}-O^{2-} nearest neighbor coordination, which mimics the calculated coordination in the hexagonal A-type form of the Ce_2O_3 sesquioxide,[11,29] in which all the Ce ions are trivalent. The geometry relaxation is coupled to a gain in the band energy (the sum of the energies of all the individual electrons; in DFT, the sum of the one-electron energies), via a decrease of the separation between the occupied Ce $4f$ states in the band gap and the O $2p$ valence band edge (hereafter referred to as the band separation, see Fig. 3), as compared to pure ceria.[11] Among the group 4b ceria compounds, the largest decrease of the band separation was found for $Ce_{0.9688}Ti_{0.0312}O_{1.9688}$ (0.27 eV),[11] which also exhibits the smallest E_f^v. In agreement with this observation, the decrease of the band separation is even larger for $Ce_{0.9688}Si_{0.0312}O_{1.9688}$ (0.30 eV). One way of quantifying the effect of local relaxation of the Ce^{3+}-M^{4+}-Va clusters is to calculate the structural relaxation energy, i.e., the effect of local strain minimization, in the

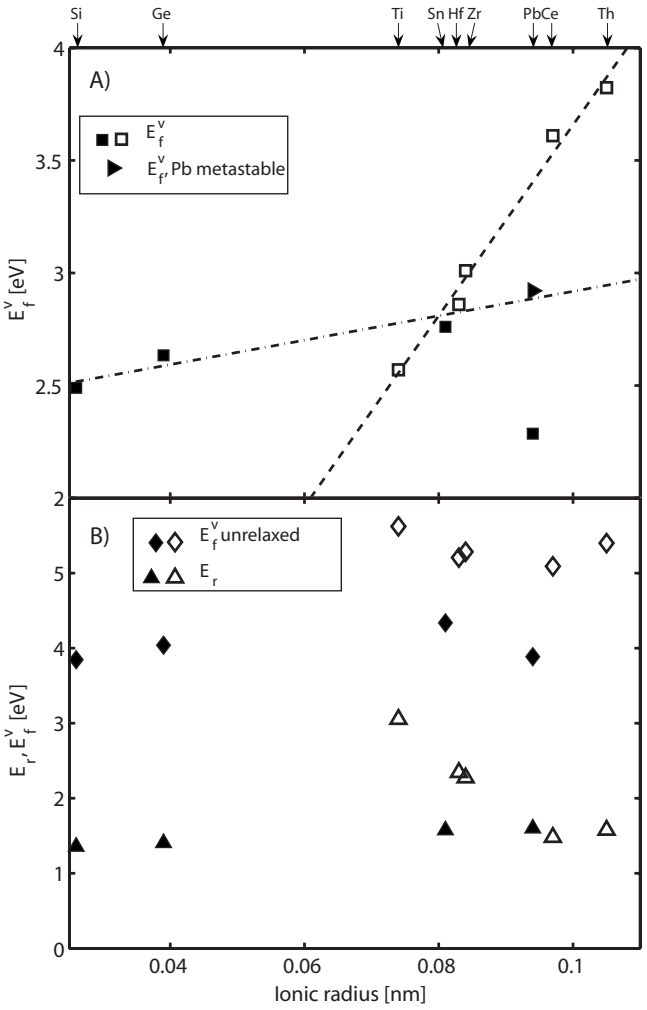

FIG. 1. (A) The vacancy formation energy (E_f^v, squares) in pure ceria as well as in ceria solid solutions $Ce_{0.9688}M_{0.0312}O_2$, where M=Si, Ge, Sn, Pb, Ti, Zr, Hf, or Th. The dashed and dot-dashed lines are given as a guide for the eyes. (B) The unrelaxed vacancy formation energy (E_f^v unrelaxed, diamonds) and the relaxation energy (E_r, triangles) in pure ceria as well as in ceria solid solutions $Ce_{0.9688}M_{0.0312}O_2$, where M=Si, Ge, Sn, Pb, Ti, Zr, Hf, or Th. In both panels (A) and (B), the group 4a elements are plotted with filled symbols and the group 4b elements with open symbols. The ionic radii (Ref. 34) either refer eightfold (Ti^{4+}, Zr^{4+}, Hf^{4+}, Th^{4+}, Sn^{4+}, and Pb^{4+}) or fourfold (Si^{4+} and Ge^{4+}) coordination of the tetravalent ions. The values for the group 4b solutes are reproduced from Ref. 11.

vacancy-containing material. Figure 1(b) shows that the unrelaxed vacancy formation energy (E_f^v unrelaxed) is markedly lower for Si^{4+} containing ceria compounds than for any of the group 4b ceria compounds. This is a consequence of the small size of the Si^{4+} ions and their strong preference to surround themselves with four oxygen ions in a tetrahedral arrangement (fourfold coordination). In the regular fluorite structure (no vacancies), the cations are surrounded by eight oxygen ions in a cubic arrangement. The Si^{4+}-O^{2-} coordination in $Ce_{0.9688}Si_{0.0312}O_2$ is illustrated in Fig. 2. In order to form the stable tetrahedron arrangement, the O^{2-} ions must leave their original fluorite lattice positions and occupy

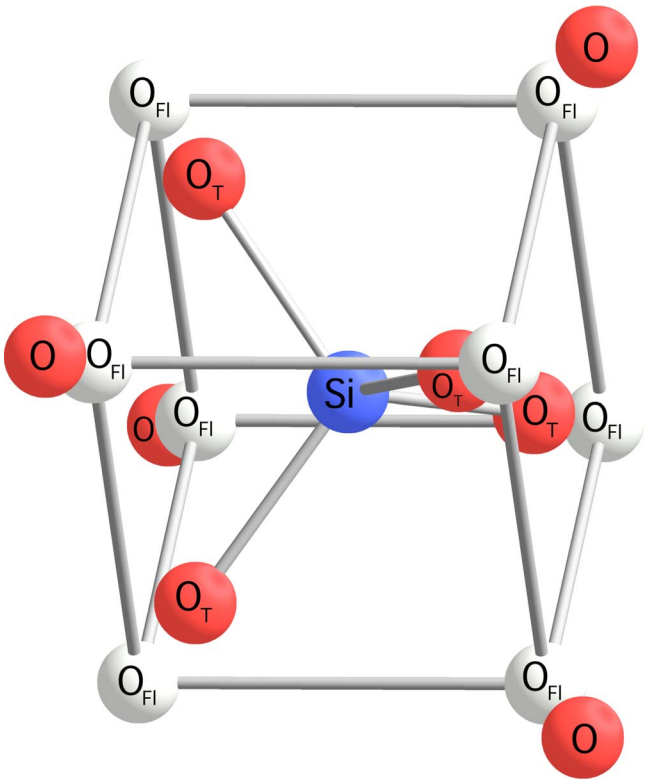

FIG. 2. (Color online) The distorted fluorite structure around the Si^{4+} solute ion in $Ce_{0.9688}Si_{0.0312}O_2$. The Si^{4+} ion is labeled by Si and the O^{2-} ions by O or O_T, where the latter denotes the O^{2-} ions that are tetrahedrally coordinated to the Si^{4+} ion. The O_T ions are connected to the Si^{4+} ion in order to highlight their tetrahedral arrangement. The original (unrelaxed) cubic arrangement of the oxygen ions is shown by the O_{Fl} ions (the Fl subscript is an abbreviation of fluorite), which are connected by bonds that form a cube around the central Si^{4+} ion.

interstitial-like sites inside the matrix. Hereafter, these ions are denoted O_T. The oxygen ions that are not a part of the tetrahedron move away from the Si^{4+} ion. The Si-O distances in the tetrahedron are $\approx$1.685 Å, which is significantly shorter than the average cation-oxygen distance in the ceria matrix (2.34 Å). The lowest-energy structural configuration of the vacancy-free material cannot be found by starting the relaxation from the positions of the ideal fluorite structure. The reason is that the local reconstruction around the +4 solute ion requires the symmetry of the eight nearest neighbor oxygen ions to be broken, which does not occur unless temperature or an external distortion is applied in the simulations. We achieve this by creating an oxygen vacancy and, after relaxing the vacancy-containing structure, the lowest-energy vacancy-free state is obtained by refilling the vacant oxygen position. The large distortions of the lattice that accompany the formation of the Si^{4+}-O^{2-} tetrahedron in the vacancy-free material explain the low values for the unrelaxed vacancy formation energy (E_f^v unrelaxed) and for the relaxation energy (E_r). For $Ce_{0.9688}Si_{0.0312}O_{1.9688}$, most of the relaxation, which for the group 4b ceria solid solutions is associated with the formation of oxygen vacancies, already takes place during the reconstruction around the Si^{4+} ion in the vacancy-free material. Figure 3 shows the projected den-

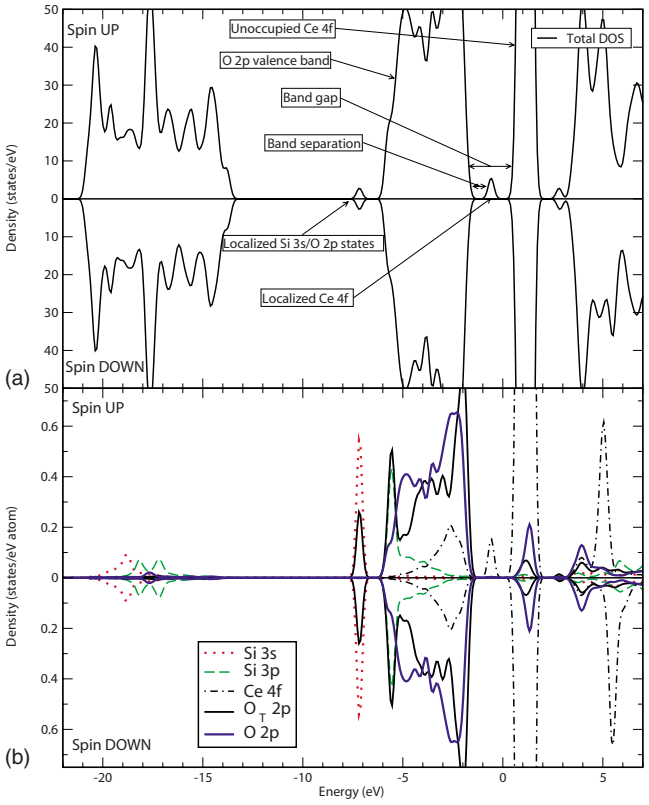

FIG. 3. (Color online) (a) The total DOS of $Ce_{0.9688}Si_{0.0312}O_{1.9688}$. (b) The PDOS of $Ce_{0.9688}Si_{0.0312}O_{1.9688}$ given per atom of each atomic species. The O_T $2p$ line shows the PDOS restricted to the O_T ions and the O $2p$ line corresponds to the PDOS summed up over all the remaining O atoms. In both (a) and (b), the highest occupied state is at 0 eV. The upper and lower panels represent the spin up and spin down channels, respectively.

sity of states (PDOS) for the Si $3s$, Si $3p$, and Ce $4f$ orbitals, given as an average over all the Si and Ce atoms in the unit cell, respectively. The O $2p$ projections are divided into the contribution from the O_T atoms and from the remaining O atoms. The O $2p$ projections that are restricted to the O_T atoms reveal that localization occurs for some O_T $2p$ states. These states are situated about 0.5–1.0 eV below the main O $2p$ band (see Fig. 3) and integration yields a total of two electrons.

The formation of the Si^{4+}-O^{2-} tetrahedron will effectively enlarge the octahedral interstitial positions in the fluorite lattice, which should lower the energy that is needed to put an oxygen ion in one of these positions. In pure ceria, our calculations predict that an energy of 4.05 eV is required to form an oxygen interstitial in the octahedral position from one of the lattice oxygen ions, i.e., a Frenkel defect. Such a high value casts some doubt upon the conclusion that a large fraction of Frenkel defects should exist in pure CeO_2.[35,36] If the oxygen ion in the octahedral interstitial position is placed next to its original lattice position, now a vacant site, it spontaneously relaxes back into this site. In $Ce_{0.9688}Si_{0.0312}O_2$, the energy needed to form a Frenkel defect is lowered to 3.09 eV. We calculated this value by placing the vacancy close to the Si^{4+} ion in the $2\times2\times2$ supercell and the oxygen ion in an octahedral interstitial site away from the vacancy. The gain in energy compared to pure ceria mainly comes from the formation of the low-energy Si^{4+}-O^{2-} tetrahedron. This mechanism may, at least partly, be responsible for the observation of interstitial oxygen ions in nanoscale CeO_2 powders.[35,36]

The properties of $Ce_{0.9688}Ge_{0.0312}O_2$ are similar to the properties of $Ce_{0.9688}Si_{0.0312}O_2$. Both the relaxed and unrelaxed vacancy formation energies are shifted slightly upwards and, equivalently, the occupied Ce f states move away from the O $2p$ valence band edge by 0.03 eV compared to $Ce_{0.9688}Si_{0.0312}O_{1.9688}$ (band separation). The Ge^{4+}-O_T distance is 1.83 Å, which is higher than for Si^{4+} but still significantly lower than the distance in the ideal fluorite structure.

The driving force to form a tetrahedral arrangement with the neighboring oxygen ions is weaker for Sn^{4+} and Pb^{4+} than for Si^{4+} or Ge^{4+}, but from the projected density of states (not shown), we conclude that there is still some localization of electrons on the oxygen ions that surround the tetravalent ions. These states are still situated below the main O $2p$ band. The localization is not restricted to the O_T ions but it involves instead all the eight nearest neighbor oxygen ions in the fluorite lattice. The average Sn^{4+}-O_T and Pb^{4+}-O_T distances are 2.07 and 2.22 Å, respectively. Unlike $Ce_{0.9688}Si_{0.0312}O_2$ and $Ce_{0.9688}Ge_{0.0312}O_2$, the vacancy formation energy for $Ce_{0.9688}Sn_{0.0312}O_2$ lies on the line that indicates the trend for the group 4b ceria compounds [dashed line in Fig. 1(a)], while the corresponding value for $Ce_{0.9688}Pb_{0.0312}O_2$ is surprisingly low [see Fig. 1(a)]. The vacancy formation energy for $Ce_{0.9688}Pb_{0.0312}O_2$ is, as a matter of fact, lower than for any of the other solute ions, in spite of the fact that Pb^{4+} has the largest ionic radius (with the exception of Th^{4+}). This is the result of a different vacancy formation mechanism in $Ce_{0.9688}Pb_{0.0312}O_2$ than for any other ceria solid solutions. For $Ce_{0.9688}M_{0.0312}O_{1.9688}$ with M being Ti, Zr, Hf, Th, Si, Ge, or Sn, the two electrons that are left behind when an oxygen atom is released from ceria localize on two nearest neighbor Ce ions, which thus transform from +4 to +3 and, due to Hund's rule, they also exhibit a localized magnetic moment of $1\mu_B/Ce^{3+}$. However, for $Ce_{0.9688}Pb_{0.0312}O_{1.9688}$, the two extra electrons instead occupy the states of mainly O $2p$ and Pb $6s$ character that are situated in the band gap 0.64 eV above the top of the O $2p$ valence band (Fig. 4). This signature is indicative of the presence of a Pb^{2+} ion. This implies that for $Ce_{0.9688}Pb_{0.0312}O_2$, the initial reduction is, in fact, due to Pb(IV)$\Rightarrow$Pb(II) rather than the usual Ce(IV)$\Rightarrow$Ce(III) reaction. The total magnetic moment of $Ce_{0.9688}Pb_{0.0312}O_{1.9688}$ is zero, while it is $2\mu_B$ for the ferromagnetically aligned solution for $Ce_{0.9688}M_{0.0312}O_{1.9688}$ (M=Ce, Ti, Zr, Hf, Th, Si, Ge, or Sn), where the reduction occurs via Ce(IV)$\Rightarrow$Ce(III). The solution for $Ce_{0.9688}Pb_{0.0312}O_{1.9688}$ with two localized Ce f electrons can be obtained as a metastable state by starting the calculation from a different magnetic and structural configuration. This solution is 0.60 eV higher in energy [triangle in Fig. 1(a)] than the ground-state solution. The metastable $Ce_{0.9688}Pb_{0.0312}O_{1.9688}$ solution predicts that the vacancy formation energy increases compared to $Ce_{0.9688}Sn_{0.0312}O_2$ and, as indicated by the dash-dotted line in Fig. 1(a), this is in

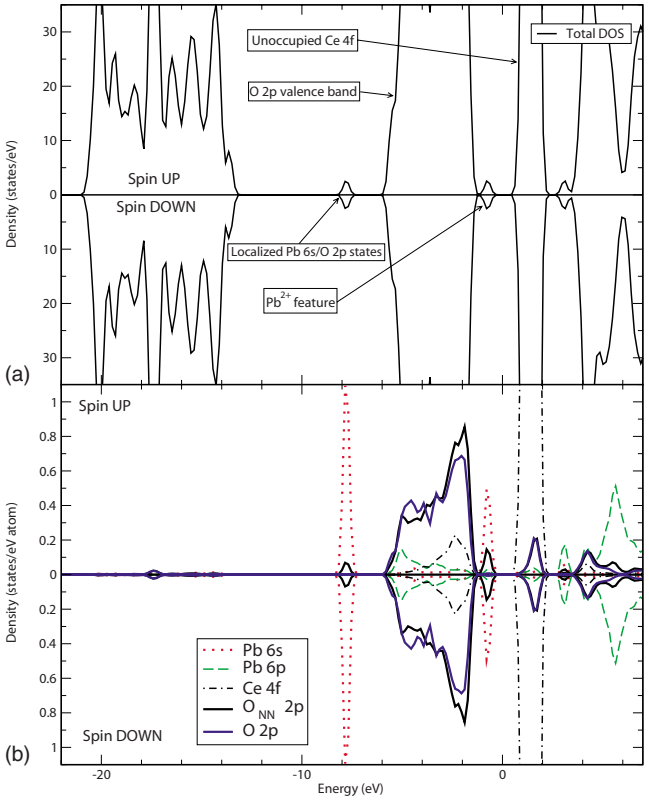

FIG. 4. (Color online) (a) The total DOS of $Ce_{0.9688}Pb_{0.0312}O_{1.9688}$. (b) The PDOS of $Ce_{0.9688}Pb_{0.0312}O_{1.9688}$ given per atom of each atomic species. The O_{NN} $2p$ line shows the PDOS restricted to the seven nearest neighbor (NN) O ions and the O $2p$ line corresponds to the PDOS summed up over all the remaining O atoms. The inset shows the states of mainly O $2p$ and Pb $6s$ character just above the main O $2p$ valence band. In both (a) and (b), the highest occupied state is at 0 eV. The upper and lower panels represent the spin up and spin down channels, respectively.

agreement with the general trend for the vacancy formation energy. For the metastable solution, the PDOS does not indicate any O $2p$ or Pb $6s$ states just above the top of the valence band, but instead localized Ce f states (two electrons) appear in the band gap. Our calculations show that the average nearest neighbor Pb-O distance (taken for the seven nearest neighbor oxygen ions) is 0.2 Å higher for the Pb^{2+} solution than for the Pb^{4+} solution, as expected from the larger size of the Pb^{2+} ion compared to the Pb^{4+} ion. We have also been able to estimate the vacancy formation energy in $Ce_{0.9688}Sn_{0.0312}O_2$ and $Ce_{0.9688}Ge_{0.0312}O_2$ according to the $M(\mathrm{IV})\Rightarrow M(\mathrm{II})$ reaction. These values are 1.31 and 2.11 eV higher in energy than for the corresponding $\mathrm{Ce(IV)}\Rightarrow\mathrm{Ce(III)}$ reactions, respectively. Since Si, Zr, Hf, and Th are very unstable in their divalent modifications, we were not able to estimate the vacancy formation energies according to the $M(\mathrm{IV})\Rightarrow M(\mathrm{II})$ reaction. Ti exists in the divalent state, e.g., in TiO.[37] Nevertheless, we were unable to calculate any accurate value for the metastable $\mathrm{Ti(IV)}\Rightarrow\mathrm{Ti(II)}$ reaction. The tendency of the M^{4+} ions to undergo reduction is directly related to the energy associated with the $MO_2\Rightarrow MO+O_2/2$ reaction. Here, MO_2 and MO refer to the ground-state structures for each metal oxide. Table I summarizes the experimental reaction enthalpies at 298 K for the Pb, Sn, Ge, and Ti oxides (there is no data for the other elements since those reactions do not occur). From these numbers, we conclude that the reaction enthalpy for Pb is significantly lower than for the other elements, which is in agreement with our theoretical prediction of the reducibility of Pb^{4+} ions in $Ce_{0.9688}Pb_{0.0312}O_2$ and the metastable character of this reduction mechanism for the other investigated solute ions.

TABLE I. ΔH is the experimental reaction enthalpy of $MO_2\Rightarrow MO+O_2/2$ at 298 K, where M=Ge, Sn, Pb, and Ti. MO_2 and MO refer to the ground-state structures for each metal oxide. The values are from Ref. 40 (Sn, Pb, and Ti) and from Ref. 41 (Ge). The calculated E_f^v values according to the $M(\mathrm{IV})\Rightarrow M(\mathrm{II})$ mechanism and the corresponding values for the $\mathrm{Ce(IV)}\Rightarrow\mathrm{Ce(III)}$ mechanism are also listed.

	Solute ion (M)			
	Ge	Sn	Pb	Ti
Expt. ΔH (eV), $MO_2\Rightarrow MO+O_2/2$	3.30	3.06	0.53	4.41
Calc. E_f^v (eV), $M(\mathrm{IV})\Rightarrow M(\mathrm{II})$	4.74	4.07	2.29	
Calc. E_f^v (eV), $\mathrm{Ce(IV)}\Rightarrow\mathrm{Ce(III)}$	2.63	2.76	2.89	2.57

Equation (2) establishes the equilibrium relation between T and P_{O_2} for CeO_{2-x} and $Ce_{0.9688}M_{0.0312}O_{2-x}$. For x =0.0312, H_f^v is known from the calculated values of E_f^v presented in Fig. 1(a) (corrected for the overestimation of the O_2 binding energy by 1.2 eV/0.5 O_2). For S_f^v, the experimental value for CeO_{2-x} (Ref. 38) can be used as a first approximation. Figure 5 shows that vacancies are most easily formed in $Ce_{0.9688}Pb_{0.0312}O_2$, followed by $Ce_{0.9688}Si_{0.0312}O_2$ and

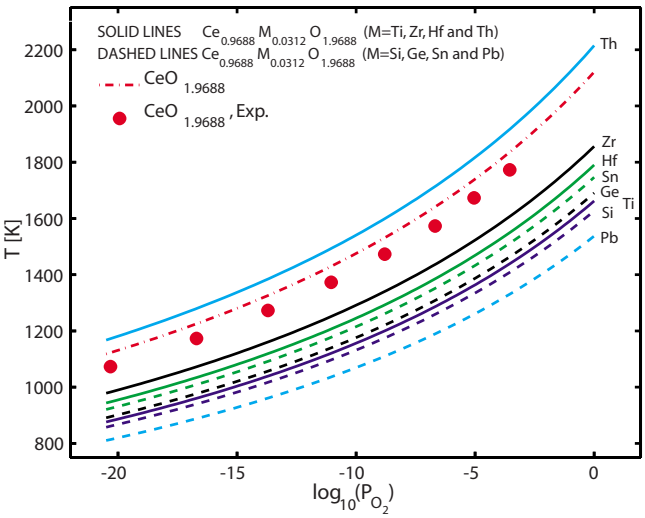

FIG. 5. (Color online) The equilibrium temperature (T) for the $Ce_{1-y}M_yO_2\Leftrightarrow Ce_{1-y}M_yO_{1.9688}+0.0156O_2$ (M=Ce, Si, Ge, Sn, Pb, Ti, Zr, Hf, or Th) reaction as a function of P_{O_2} for y=0.0312. The experimental data (circles) are from Ref. 42. The solute atom, M, is indicated at the right end points of each line. The solid lines refer to the group 4b elements and the dashed lines refer to the group 4a elements.

$Ce_{0.9688}Ti_{0.0312}O_2$ (the $Ce_{0.9688}Pb_{0.0312}O_2$ number refers to the $M(IV) \Rightarrow M(II)$ reaction). $Ce_{0.9688}Th_{0.0312}O_2$ is the only compound that increases the reduction temperature. Moreover, $Ce_{0.9688}Si_{0.0312}O_2$, $Ce_{0.9688}Ge_{0.0312}O_2$, $Ce_{0.9688}Sn_{0.0312}O_2$, and $Ce_{0.9688}Pb_{0.0312}O_2$ all have lower reduction temperatures than $Ce_{0.9688}Zr_{0.0312}O_2$, which represents the current state of the art OSC material (not necessarily with this particular Zr concentration).

B. Migration barriers and defect binding (association) in $Ce_{0.9688}M_{0.0312}O_{1.9688}$

The oxygen diffusivity, which, for example, determines how fast the bulk ceria material can exchange oxygen with the surrounding environment, is influenced by interactions between the dissolved +4 ions and the oxygen vacancies. The diffusivity is governed by the activation energy for diffusion, which is identified as the sum of the migration barrier for moving an oxygen ion from one lattice site to a neighboring vacant site (E_m) and the binding energy between vacancies and tetravalent solutes. We estimated E_m [Fig. 6(a)] by calculating the energy that is needed to place an oxygen ion in the saddle point position that is situated next to the +4 solute ion in the $2\times2\times2$ supercell model of $Ce_{0.96880}M_{0.0312}O_{1.9688}$. The saddle point is taken halfway between the oxygen sites involved in the diffusion process.[39] The migrating oxygen ion was only allowed to relax in the directions perpendicular to the migration path, while the remaining ions were fully relaxed. Compared to pure ceria, the barrier decreases significantly for Sn^{4+} and Pb^{4+}, which is understood from the fact that the small size of these ions allows a simple passage through the saddle point. The barrier for the saddle point next to a Pb^{2+} ion [remember the $Pb(IV) \Rightarrow Pb(II)$ reaction mechanism] is much higher than for the Pb^{4+} case (1.52 eV compared to 0.27 eV), which is due to the large size of the Pb^{2+} ion. This implies that the diffusing oxygen ions in Pb-doped ceria would avoid the migration paths involving saddle points close to the Pb^{2+} ions. One may speculate that the Pb^{2+} barrier is lowered by an (instantaneous) electronic transition from Pb^{2+} to Pb^{4+}, accompanied by the formation of two Ce^{3+} ions, when an oxygen ion passes through the saddle point. Our calculations show that such a reaction is energetically favorable. Even though both the Si^{4+} and the Ge^{4+} ions are small, their tetrahedral oxygen coordination results in migration barriers that are of the same magnitude as for the larger Sn^{4+} and Pb^{4+} ions. We note that the migration barriers that enter the activation energy for diffusion correspond to an effective bulk barrier and should not be directly identified with the barrier close to the M^{4+} ions, at least not for low concentration of solute ions.

Oxygen vacancies bind to the +4 solute ions and Fig. 6(b) contains our calculated binding energies. The Pb^{2+}-Va binding energy is approximately 0.1 eV higher than for Pb^{4+}-Va [Pb^{4+}-Va is shown in Fig. 6(b)]. For small solute concentrations, defect binding will increase the activation energy for diffusion and thus decrease the diffusivity of oxygen ions. Due to overlapping interaction fields of the solute ions, this effect should decrease for increasing solute concentrations.

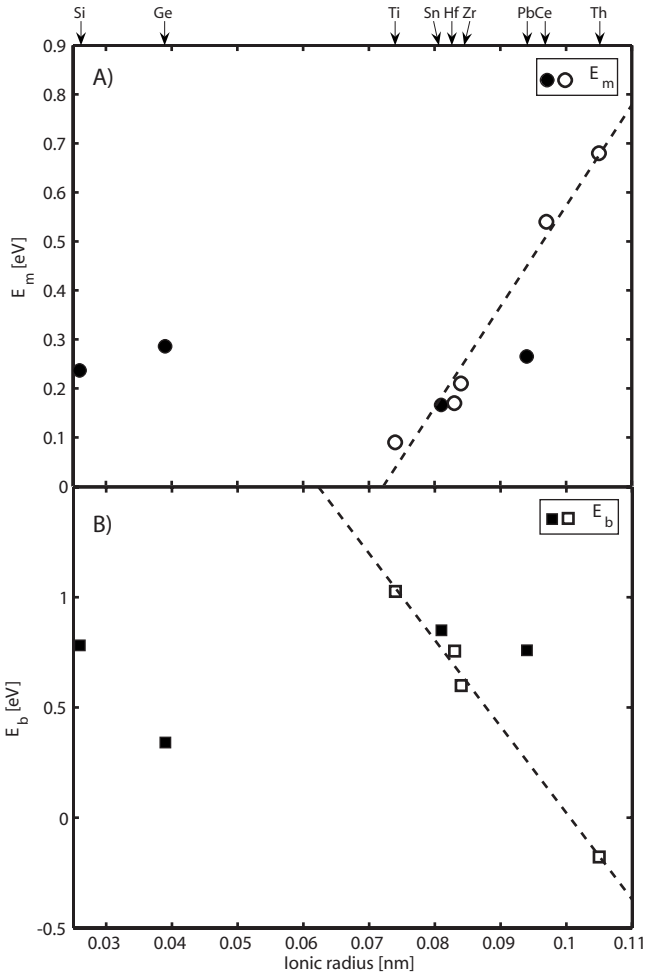

FIG. 6. (A) The migration barrier (E_m, circles) in pure ceria as well as in ceria solid solutions $Ce_{0.9688}M_{0.0312}O_{1.9688}$, where M = Ti, Zr, Hf, Th, Si, Ge, Sn, and Pb. (B) The binding energy of +4 solute ions and vacancies (E_b, squares). In both panels, the values for Ti, Zr, Hf, and Th are from Ref. 11. Filled symbols represent the group 4a elements and the open symbols represent the group 4b elements. The dashed lines are given as a guide for the eyes.

C. Dissolution of tetravalent solutes (M^{4+}), $Ce_{0.9688}M_{0.0312}O_2$

The solution energy (E_s) of +4 ions in ceria determines the stability of the solid solution phases with respect to phase separation into the constituent oxides. Figure 7 shows the calculated values of E_s for one +4 ion in the $2\times2\times2$ supercell ($Ce_{0.9688}M_{0.0312}O_2$). The rutile structure was used as the reference state of Si^{4+}, Ge^{4+}, Sn^{4+}, and Pb^{4+}. We note that the ground-state structures of SiO_2 and GeO_2 is of α-quartz type and the corresponding solution energies in Fig. 7 should thus be shifted slightly upward. For Th^{4+}, the fluorite structure was used as the reference state, while we used the anatase structure for Ti^{4+} and the monoclinic baddeleyite structure for Hf^{4+} and Zr^{4+}. In particular, we emphasize the excellent agreement with experimental data for Zr^{4+}.[43] The solution energies exhibit an approximately linear dependence on the ionic radii. Ions of similar size as Ce^{4+} are easy to dissolve in the CeO_2 matrix, while small ions are more difficult to dissolve. Since all the solution energies are positive, the solid

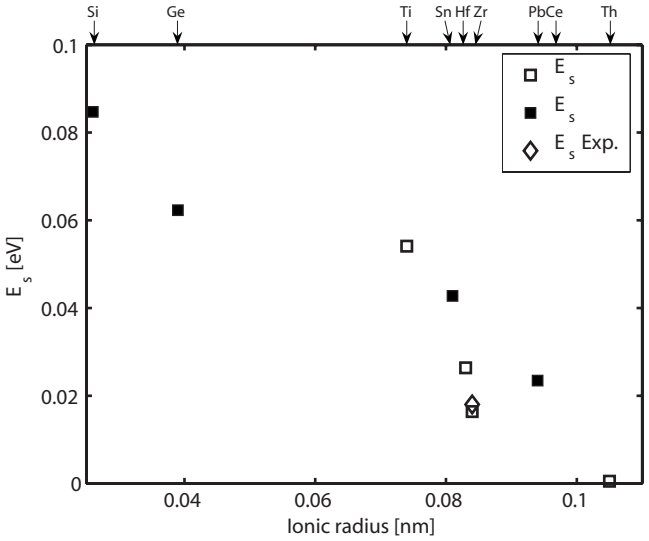

FIG. 7. The solution energy (E_s, squares) in pure ceria as well as in ceria solid solutions $Ce_{0.9688}M_{0.0312}O_2$, where M=Si, Ge, Sn, Pb, Ti, Zr, Hf, or Th. The group 4a elements are plotted with filled symbols, and the group 4b elements with open symbols. The values for the group 4b solutes are reproduced from Ref. 11. The experimental solution energy is from Ref. 43.

solutions will be metastable at low temperature, but at high temperature, entropy provides a stabilizing contribution. Nevertheless, there will be a strong tendency to phase separate for the small solute ions. From Fig. 7, we conclude that both Sn^{4+} and Pb^{4+} are easier to dissolve than Ti^{4+}. At the same time, Sn^{4+} and Pb^{4+} yield similar or even lower vacancy formation energies, i.e., they have higher reducibility. Within each group (4a and 4b), there is an inverse relation between high solution energy and high reactivity [low vacancy formation energy, compare Fig. 1(a)]. The unique properties of Pb make it an exception, i.e., both the solution energy and the vacancy formation energy are quite low.

D. Vacancy formation and M^{4+} solution energies in $Ce_{1-y}M_yO_2$

In order to clarify how the solution energy and the vacancy formation energy depend on the concentration of tetravalent solutes, we have studied $Ce_{1-y}M_yO_2$ with M being Ti, Zr, Hf, Th, Si, Ge, or Sn and y=0.0312, 0.0625, or 0.25. The y=0.0312 case has been discussed extensively in the preceding sections. In order to have the same vacancy concentration for every y, we have used the $2\times2\times2$ supercell setup, not only for y=0.0312 but also for y=0.0625 and y =0.25. In the latter two cases, we have to make some assumption about the distribution of the tetravalent solutes on the Ce sublattice. The detailed distribution is not known from experiments and, moreover, due to slow cationic diffusion, the distribution does, in general, not correspond to complete equilibrium. For each y, we tried two different models that mimic the clustering and homogeneous (equally spaced) distribution of the solute ions. In the clustering model, for y =0.0625, the two solute ions in the supercell are assumed to be nearest neighbors, and for y=0.25, the solute ions are assumed to occupy one separate (100) plane (the solute ions are nearest neighbors also in this case). The latter model mimics the planar type of ordering pattern suggested for $CeZrO_2$ in Ref. 44. The models for the homogeneous distribution were constructed by placing the solute ions at equal distances from each other in the $2\times2\times2$ supercell. In order to find the relaxed vacancy-free structures, we used the following technique. First, we removed an oxygen atom and relaxed the structure and then we replaced the oxygen atom again, as it was described for single Si^{4+} solutes in Sec. III A. If we start the relaxation from the original fluorite lattice positions, we do not reach the ground-state structure. This conclusion applies to M=Ti, Si, Ge, and Sn, while the ground-state structure for M=Zr, Hf, and Th was obtained by conventional relaxation schemes. Our DFT calculations show that the homogeneous distribution of solute ions is more stable than the clustered state (Pb is an exception). In order to illustrate this property, Fig. 8 shows the energy difference between the two distribution models for $Ce_{0.9375}M_{0.0625}O_2$, which is equivalent to the binding energy of +4 solute ions (negative values mean that the ions do not want to have each other as nearest neighbors). The energy difference between the two distribution models is the largest for Si^{4+}, Ge^{4+}, Sn^{4+}, and Ti^{4+} because these ions (referred to as group A in the following) distort the original fluorite structure to a much larger extent than the Zr^{4+}, Hf^{4+}, and Th^{4+} ions (referred to as group B in the following). The large distortions for group A follows from the tendency to form a fourfold M^{4+}-O^{2-} coordination, e.g., the formation of the tetrahedral M^{4+}-O^{2-} environment in $Ce_{0.9688}Si_{0.0312}O_2$ and $Ce_{0.9688}Ge_{0.0312}O_2$, instead of the eightfold oxygen coordination in the fluorite crystal structure. We recall that SiO_2, GeO_2, SnO_2, and TiO_2 (group A) all prefer the rutile crystal structure (fourfold coordination) rather than the fluorite structure or any other closely related structure. The stability of the rutile and fluorite crystal structures is reversed for ZrO_2, HfO_2, and ThO_2 (group B). If the +4 solutes in group A are situated close to each other, the redistribution of the surrounding oxygen ions into the tetrahedral coordination is more difficult than for the homogeneous solute distribution, which explains the energetic preference for the latter distribution. Pb^{4+} is the only solute ion that prefers the clustered distribution, even though this is only marginally more stable than the homogeneous distribution. Since PbO_2 is more stable in the rutile structure than in the fluorite structure, we classify Pb as a group A element, which is also consistent with the results discussed below.

The volume relaxation for $Ce_{0.75}M_{0.25}O_2$ is plotted in Fig. 9. These values refer to the lowest-energy structures, i.e., the homogeneous distribution of solutes. At first glance the data points seem rather scattered, but if the group A and group B solutes are treated separately, an almost linear function of the ionic radii emerges for group B (see the dashed line). The trend is not as obvious for group A, but it is apparent that it deviates from the group B behavior. In this context, we recall that group A could, in fact, be further subdivided since the ground-state structure of both SiO_2 and GeO_2 is the α-quartz structure. The reason for this is the high degree of structural relaxation for group A compared to group B, which, in fact, leads to the formation of a new ordered crystal structure for

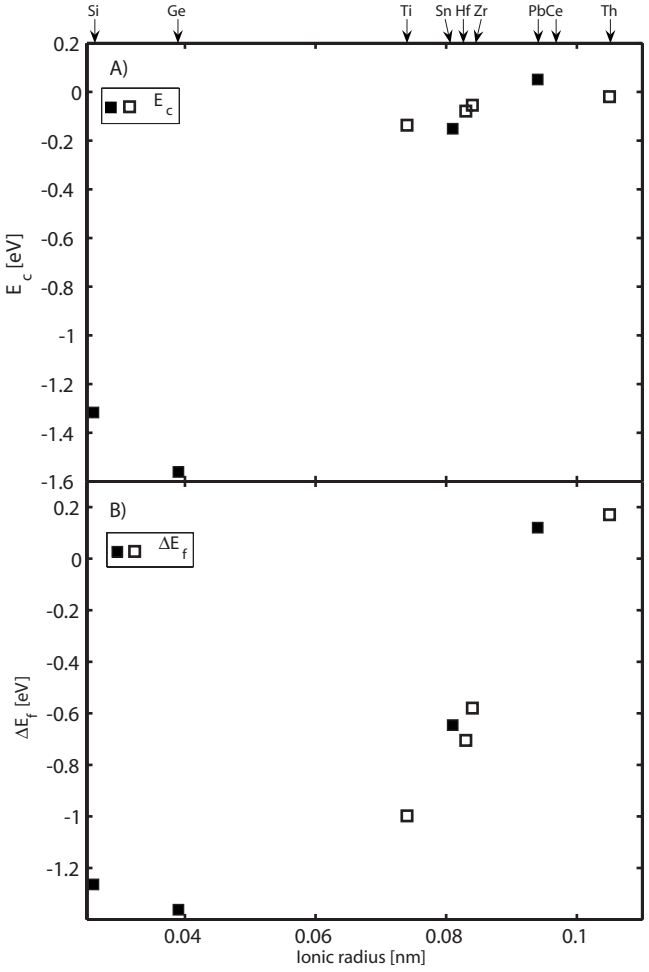

FIG. 8. (A) The energy difference between the homogeneous and the clustering distribution models of the +4 solute ions in $Ce_{0.9375}M_{0.0625}O_2$ (M=Ti, Zr, Hf, Th, Si, Ge, Sn, and Pb), based on the $2\times2\times2$ supercell (E_c), which is equivalent to the binding energy of the +4 solute ions. Negative values imply that the +4 ions do not want to have each other as nearest neighbors. (B) The difference in the vacancy formation energy between the clustering and homogeneous distribution models of $Ce_{0.9375}M_{0.0625}O_2$. Negative values mean that it is easier to form vacancies in the clustering model.

the group A compounds that is closely related to the original fluorite structure. The new crystal structure is formed by displacing half of the oxygen ions in the oxygen cube that surrounds each M^{4+} ion in the fluorite structure toward the M^{4+} ion itself, while the remaining oxygen ions move away from the M^{4+} ion. This results in a fourfold tetrahedronlike environment around each M^{4+} ion. This relaxation pattern is equivalent to the structure in Fig. 2. In the homogeneous structure model, the M^{4+} ions form a cubic sublattice and thus the displaced oxygen ions will also form a separate sublattice of cubic symmetry. All the compounds that belong to group A form ordered superstructures of the type described above, which explains their special behavior compared to the group B compounds in Fig. 9.

The calculated concentration dependence of the solution energies for the homogeneous distribution of solute ions is

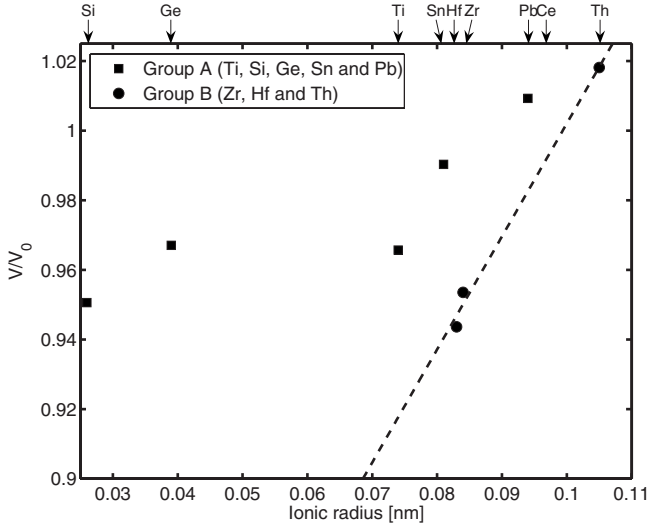

FIG. 9. The relative volume relaxation (V/V_0, where V_0 is the calculated volume of pure ceria) for $Ce_{0.75}M_{0.25}O_2$ (M=Ti, Zr, Hf, Th, Si, Ge, Sn, and Pb) as a function of the solute ionic radius for the homogeneous distribution of solute ions (see text). The solutes can be divided into two groups, containing Ti, Si, Ge, Sn, and Pb (group A) and Zr, Hf, and Th (group B). Within group B, there is an almost linear relation, as indicated by the dashed line.

shown in Fig. 10. There is an excellent agreement with experiments for Zr^{4+},[43] which validates the present modeling approach. The highest and the lowest solution energies are obtained for Si and Th, respectively. For $Ce_{0.75}M_{0.25}O_2$ (y=0.25) with M being Ti, Si, Ge, Sn, and Pb, the solution energy is lower than suggested by a linear extrapolation from the y=0.0312 and y=0.0625 values, which follows from the large structural relaxation and the formation of an ordered superstructure, as described in the previous paragraph. From Fig. 8(a), we conclude that the solution energies for the clustered distribution would be even higher than for the homogeneous distribution of solute ions.

Figure 11 shows how the vacancy formation energy depends on the concentration of solute ions for the homoge-

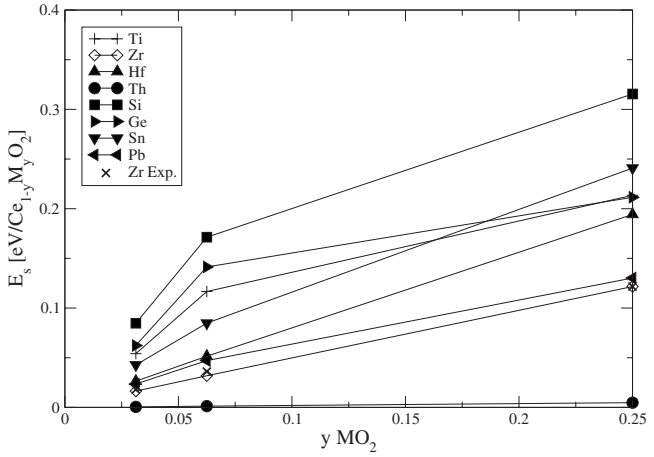

FIG. 10. The concentration dependence of the solution energy of TiO_2, ZrO_2, HfO_2, ThO_2, SiO_2, and SnO_2 in CeO_2, i.e., $Ce_{1-y}M_yO_2$ with M=Ti, Zr, Hf, Th, Si, and Sn.

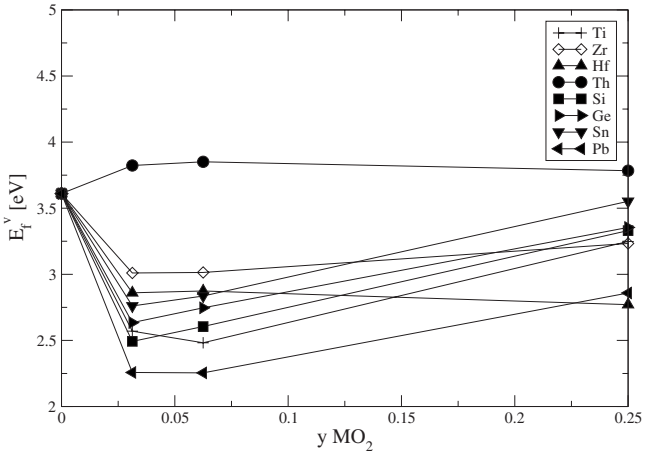

FIG. 11. The concentration dependence of the vacancy formation energy in $Ce_{1-y}M_yO_2$ with M being Ti, Zr, Hf, Th, Si, Ge, Sn, and Pb.

neous distribution of solutes. Up to $y=0.0312$, the vacancy formation energies decrease (except for Th^{4+}), but between $y=0.0312$ and $y=0.25$, this trend is reversed and the energies are of equal magnitude or even higher than for the low-concentration range ($y=0.0312$). Zhou *et al.* measured the reduction energy (vacancy formation energy) for $Ce_{1-y}Zr_yO_2$ and they reported a very weak concentration dependence,[16] in agreement with our theoretical predictions. The experimental value of E_f^v for $Ce_{1-y}Zr_yO_2$ is ≈ 2.72 eV,[15] which is somewhat lower than our theoretical result especially if the overestimation of the binding energy of O_2 molecules is taken into account. The reason for this partial discrepancy will be further analyzed. The increase of the vacancy formation energy between $y=0.0312$ and $y=0.25$ is most significant for Ti^{4+}, Si^{4+}, Ge^{4+}, Sn^{4+} and Pb^{4+}, which correlates with the large structural relaxations and the formation of ordered superstructures for these compounds (group A). From Fig. 8(b), we conclude that the vacancy formation energy is markedly lower for clustered solute ions than for the homogeneous distribution in Fig. 11, which correlates with the higher solution energies for these compounds compared to the homogeneous solute distribution.

For both $y=0.0625$ and $y=0.25$, reduction occurs via the Ce(IV)⇒Ce(III) reaction for all the solute ions except for Pb^{4+}, which is reduced according to Pb(IV)⇒Pb(II). In the $2\times2\times2$ supercell model of $Ce_{0.9375}Ti_{0.0625}O_2$, one could imagine the Ti(IV)⇒Ti(III) reaction to be more favorable than the Ce(IV)⇒C(III) reaction (the other solute ions are unstable in their trivalent modification), but according to our calculations, the latter reaction always occurs in the initial reduction step. We checked if this conclusion is changed by the application of a Hubbard U term between 2 and 6 eV for the Ti $3d$ orbitals, but the Ce(IV)⇒C(III) reaction was still the least endothermic.

IV. CONCLUSIONS

Using density functional theory calculations, we have shown that small amounts of dissolved SiO_2, GeO_2, SnO_2, or PbO_2 improve the reducibility of ceria (CeO_2), as quantified by the decrease of the vacancy formation energy. The reason for this is the favorable geometry relaxation of the Ce^{3+}-M^{4+}-Va clusters in the reduced samples, which results in a gain in the band energy due to the motion of the localized Ce $4f$ states in the band gap toward the valence band edge, i.e., the decrease of the band separation. The reducibility increases in the sequence of CeO_2-SnO_2, CeO_2-GeO_2, and CeO_2-SiO_2. For all these materials, the vacancy formation energy is lower than for the current state of the art CeO_2-ZrO_2 materials. The group 4a solutes tend to form a tetrahedral arrangement with the surrounding +4 ions; in particular, this tendency is strong for Si^{4+} and Ge^{4+}, which is accompanied by the localization of electrons on the nearest neighbor oxygen ions. This yields highly distorted structures for CeO_2-SiO_2 and CeO_2-GeO_2. CeO_2-PbO_2 is unique in the sense that the initial reduction occurs by Pb(IV)⇒Pb(II) instead of the usual Ce(IV)⇒Ce(III) reaction. Among all the investigated ceria compounds, CeO_2-PbO_2 has the highest reducibility. For low solute concentrations, there is an inverse relation between high reducibility and the solution energy of tetravalent solutes. The +4 solute ions influence the diffusivity of oxygen ions in two ways: by decreasing the migration barrier close to the solute ions and by forming bound defect complexes with the oxygen vacancies. The former contribution decreases the activation energy for diffusion and thus the diffusivity of oxygen ions, while the latter works in the opposite direction. The height of the migration barrier and the defect binding energy are inversely related. We have also studied how the solution energy and the reducibility depend on the concentration of Ti, Zr, Hf, Th, Si, Ge, Sn, and Pb solute ions. Starting from pure ceria, there is an initial decrease of the reduction energy, after which it remains almost constant (Zr, Hf, and Th) or increases slightly (Ti, Si, Ge, Sn, and Pb) for high solute concentrations. The increase is a consequence of the formation of an ordered superstructure from the defective fluorite structure. The solution energies increase monotonously with concentration. Our calculations also reveal that the solutes do not want to have each other as nearest neighbors and therefore favor a homogeneous distribution (Pb is an exception); in particular, this effect is important for ceria that contains Si^{4+} and Ge^{4+} ions. The formation of metastable clusters of +4 solute ions decreases the vacancy formation energy significantly.

ACKNOWLEDGMENTS

The Swedish Foundation for Strategic Research (SSF) and the Swedish Research Council (VR) are acknowledged for financial support. The Swedish National Infrastructure for Computing (SNIC) is acknowledged for computer resources. One of the authors (D.A.A.) gratefully thanks the Center for Computational Thermodynamics (CCT), the MATOP program, and the Brinell centre for support.

[1] A. Trovarelli, *Catalysis by Ceria and Related Materials* (Imperial College Press, London, 2002).
[2] J. Kaspar, P. Fornasiero, and M. Graziani, Catal. Today **50**, 285 (1999).
[3] S. Park, J. M. Vohs, and R. J. Gorte, Nature (London) **404**, 265 (2000).
[4] B. C. H. Steele and A. Heinzel, Nature (London) **414**, 345 (2001).
[5] T. Hibino, A. Hashimoto, T. Inoue, J.-I. Tokuno, S.-I. Yoshida, and M. Sano, Science **288**, 2031 (2000).
[6] N. V. Skorodumova, S. I. Simak, B. I. Lundqvist, I. A. Abrikosov, and B. Johansson, Phys. Rev. Lett. **89**, 166601 (2002).
[7] P. Fornasiero, R. Dimonte, G. R. Rao, J. Kaspar, S. Meriani, A. Trovarelli, and M. Graziani, J. Catal. **151**, 168 (1995).
[8] T. Murota, T. Hasegawa, S. Aozasa, H. Matsui, and M. Motoyama, J. Alloys Compd. **193**, 298 (1993).
[9] M. Boaro, A. Trovarelli, J.-H. Hwang, and T. O. Mason, Solid State Ionics **147**, 85 (2002).
[10] J. A. Rodriguez, J. C. Hanson, J.-Y. Kim, G. Liu, A. Iglesias-Juez, and M. Fernández-Garía, J. Phys. Chem. B **107**, 3535 (2003).
[11] D. A. Andersson, S. I. Simak, N. V. Skorodumova, I. A. Abrikosov, and B. Johansson, Appl. Phys. Lett. **90**, 031909 (2007).
[12] F. Zamar, A. Trovarelli, C. De Leitenburg, and G. Dolcetti, Stud. Surf. Sci. Catal. **101**, 1283 (1996).
[13] T. Baidya, A. Gayen, M. S. Hegde, N. Ravishankar, and Loic Dupont, J. Phys. Chem. B **110**, 5262 (2006).
[14] G. Dutta, U. V. Waghmare, T. Baidya, M. S. Hegde, K. R. Priolkar, and P. R. Sarode, Chem. Mater. **18**, 3249 (2006).
[15] P. R. Shah, T. Kim, G. Zhou, P. Fornasiero, and R. J. Gorte, Chem. Mater. **18**, 5363 (2006).
[16] G. Zhou, P. R. Shah, T. Kim, P. Fornasiero, and R. J. Gorte, Catal. Today **123**, 86 (2007).
[17] B. M. Reddy, A. Khan, P. Lakshmanan, M. Aouine, S. Loridant, and J.-C. Volta, J. Phys. Chem. B **109**, 3355 (2005).
[18] B. M. Reddy and A. Khan, Catal. Surv. Asia **9**, 155 (2005).
[19] E. Rocchini, A. Trovarelli, J. Llorca, G. W. Graham, W. H. Weber, M. Maciejewski, and A. Baiker, J. Catal. **194**, 461 (2000).
[20] E. Rocchini, M. Vicario, J. Llorca, C. de Leitenburg, G. Dolcetti, and A. Trovarelli, J. Catal. **211**, 407 (2002).
[21] R. Lin, M.-F. Luo, Y.-J. Zhong, Z.-L. Yan, G.-Y. Liu, and W.-P. Liu, Appl. Catal., A **255**, 331 (2003).
[22] R. Lin, Y.-J. Zhong, M.-F. Luo, and W.-P. Liu, Indian J. Chem. Sect. A **40**, 36 (2001).
[23] G. Kresse and J. Hafner, Phys. Rev. B **48**, 13115 (1993).
[24] G. Kresse and J. Furthmüller, Comput. Mater. Sci. **6**, 15 (1996).
[25] G. Kresse and J. Furthmüller, Phys. Rev. B **54**, 11169 (1996).
[26] G. Kresse and D. Joubert, Phys. Rev. B **59**, 1758 (1999).
[27] P. E. Blöchl, Phys. Rev. B **50**, 17953 (1994).
[28] S. L. Dudarev, G. A. Botton, S. Y. Savrasov, C. J. Humphreys, and A. P. Sutton, Phys. Rev. B **57**, 1505 (1998).
[29] D. A. Andersson, S. I. Simak, B. Johansson, I. A. Abrikosov, and N. V. Skorodumova, Phys. Rev. B **75**, 035109 (2007).
[30] H. J. Monkhorst and J. D. Pack, Phys. Rev. B **13**, 5188 (1976).
[31] P. E. Blöchl, O. Jepsen, and O. K. Andersen, Phys. Rev. B **49**, 16223 (1994).
[32] M. Nolan, S. C. Parker, and G. W. Watson, Surf. Sci. **595**, 223 (2005).
[33] M. A. Panhans and R. N. Blumenthal, Solid State Ionics **60**, 279 (1993).
[34] R. D. Shannon, Acta Crystallogr., Sect. A: Cryst. Phys., Diffr., Theor. Gen. Crystallogr. **32**, 751 (1976).
[35] E. Mamontov and E. Egami, J. Phys. Chem. Solids **61**, 1345 (2000).
[36] E. Mamontov, E. Egami, B. Brezny, M. Koranne, and S. Tyagi, J. Phys. Chem. B **104**, 11110 (2000).
[37] D. A. Andersson, P. A. Korzhavyi, and B. Johansson, Phys. Rev. B **71**, 144101 (2005).
[38] M. A. Panhans, R. N. Blumenthal, and J. E. Garnier, J. Phys. Chem. Solids **36**, 1213 (1975).
[39] D. A. Andersson, S. I. Simak, N. V. Skorodumova, I. A. Abrikosov, and B. Johansson, Proc. Natl. Acad. Sci. U.S.A. **103**, 3518 (2006).
[40] *Thermochemical Properties of Inorganic Substances*, edited by I. Barin and O. Knacke (Springer, Berlin, 1977).
[41] *CRC Hanbook of Chemistry and Physics*, 87th ed., edited by David R. Lide (Taylor & Francis, Boca Raton, 2007).
[42] B. M. Reddy, A. Kahn, P. Lakshmanan, M. Aouine, S. Loridant, and J.-C. Volta, J. Phys. Chem. B **109**, 3355 (2005).
[43] A. Navrotsky, P. Simomcic, H. Yokokawa, W. Chen, and T. Lee, Faraday Discuss. **134**, 10 (2006).
[44] J. C. Conesa, J. Phys. Chem. B **107**, 8840 (2003).